

Strasser, M., Ikehara, K., Everest, J., and the Expedition 386 Scientists *Proceedings of the International Ocean Discovery Program* Volume 386 publications.iodp.org







Contents

- 1 Abstract
- 1 Introduction
- 3 Materials and methods
- **5** Results
- 8 Acknowledgments
- 8 References

Keywords

International Ocean Discovery Program, IODP, *Kaimei*, Missionspecific platform, Expedition 386, Japan Trench Paleoseismology, Site M0090

References (RIS)

MS 386-201

Received 20 May 2025 Accepted 11 August 2025 Published 29 October 2025

Data report: major element oxides and CI of volcanic glass shards at Japan Trench Site M0090, IODP Expedition 386: searching for the To-Cu marker volcanic ash¹

Susanne M. Straub²

- ¹ Straub, S.M., 2025. Data report: major element oxides and Cl of volcanic glass shards at Japan Trench Site M0090, IODP Expedition 386: searching for the To-Cu marker volcanic ash. In Strasser, M., Ikehara, K., Everest, J., and the Expedition 386 Scientists, Japan Trench Paleoseismology. Proceedings of the International Ocean Discovery Program, 386: College Station, TX (International Ocean Discovery Program). https://doi.org/10.14379/iodp.proc.386.201.2025
- ²Lamont-Doherty Earth Observatory, Columbia University, USA. Correspondence author: smstraub@ldeo.columbia.edu

Abstract

Major element oxides and Cl of dispersed (invisible to the naked eye) volcanic glass shards were measured in clastic sediments of the central Japan Trench recovered at Site M0090 during International Ocean Discovery Program Expedition 386, Japan Trench Paleoseismology. The glass shards were extracted from two giant piston cores, Core 386-M0090B-1H (Sections 1H-15, 80 cm, to 1H-14, 50 cm) and Core 386-M0090D-1H (Sections 1H-14, 0 cm, to 1H-13, 50 cm), which together represent 180 cm of the sediment. High-resolution sampling with 1 and 5 cm spacing (65 samples) aimed to better define the stratigraphic position of the To-Cu marker ash (~6000 y before present), which had previously been identified within this interval. Electron microprobe analysis reveals low-K volcanic glasses (<1.5 wt% K₂O; ~67% of the glass data) and medium- and high-K glasses (>1.5 to 5 wt% K_2O ; ~33% of the glass data) in all 65 samples. The low-K volcanic glasses display the typical compositional characteristics of volcanic glass from the Towada volcano in Northern Honshu and may be mostly of To-Cu origin. The medium- and high-K glasses are likely an assortment of volcanic glasses produced during various Holocene and Pleistocene explosive eruptions of the Honshu arc volcanoes. Variation in grain size fraction, magnetic susceptibility, bulk density, and natural gamma radiation of the sediment sequence sampled suggests that all glass shards were emplaced in turbidite flow either syn- or posteruptively with a major explosive eruption of the Towada volcano.

1. Introduction

The goal of International Ocean Discovery Program (IODP) Expedition 386 was to obtain a long-term record of earthquake-triggered event deposits in the Japan Trench (Strasser et al., 2024). To this purpose, a total of 29 giant piston cores, 20-40 m in length, were recovered from 11 sediment-filled basins on the bottom of the Japan Trench (Figure F1). The cored sediment consists mostly of clay, silty clay, and clayey silt, which is interspersed with centimeter- to meter-thick coarser grained layers rich in silt and very fine sand (Strasser et al., 2024). In its entirety, most of the cored trench sediments are redeposited. Redeposition, together with the young Holocene to very late Pleistocene age of the sediments (<28,000 y; Strasser et al., 2024) and the hadal water depths (7745–8023 m) below the calcite-compensation depth, limits biostratigraphic and paleomagnetic dating of these deposits. Therefore, marker fallout ash beds produced by the Holocene and late Pleistocene large-magnitude explosive eruptions (volcanic explosivity index [VEI] ≥ 5 [Newhall and Self, 1982]) from the Honshu arc volcanoes (e.g., Machida, 2002; Aoki et al., 2008; Kimura et

al., 2015; Ikehara et al., 2017) play a vital role in the intersite stratigraphic correlation (Satoguchi et al., 2024; Strasser et al., 2024).

Postcruise work identified several marker ash beds in Expedition 386 cores, such as the To-Cu (5986-5899 cal y BP), Hj-O (12,000 y), To-H (15,515-15,895 y), and As-K $(16,619 \pm 74 \text{ y})$ (Satoguchi et al., 2024). In addition, marker layers As-B (108 CE) and H-FP (555-615 CE) were tentatively identified (Satoguchi et al., 2024). Among these marker beds, the fallout ash deposits from Towada volcano in North Honshu are important because they have distinct low-K, high-silica compositions and are important middle Holocene to late Pleistocene age markers of the larger Tohoku region (northern part of North Honshu) (e.g., Machida, 1999b; Ishimura and Hiramine, 2020). The Towada marker ash beds range from the young, historic Towada-a (To-a) tephra (915 CE) to the To-Cu ash produced by a VEI = 5 explosive eruption at 5986–5899 cal y BP (McLean et al., 2018), and the To-H (12,200–14,000 BP) and Towada-Ofudo (To-Of) tephras (ca. 33 ka), which were produced by larger VEI > 7 eruptions (Machida, 1999a). Fallout marker beds To-a, To-Cu, and To-H have previously been identified in the marine sediments east of Tohoku (Ikehara et al., 2017; Matsu'ura and Komatsubara, 2018). The To-Cu ash fallout distribution is best investigated from distal and proximal outcrops across North Honshu (Ishimura and Hiramine, 2020) and marine ash beds offshore northern North Honshu (Ikehara et al., 2017; Matsu'ura and Komatsubara, 2018). The explosive To-Cu eruption had three phases that produced first the most widely spread Chuseri pumice (Cu) (which recently has even been reported from mainland China [Sun et al., 2021]), followed by the Kanegasawa pumice (Kn) and Utarube ash (Ut) (Ishimura and Hiramine, 2020). Isopach maps based on multiple subaerial outcrops across Honshu indicate a south-to-southeast main axis of the To-Cu fallout ash and thicknesses of several centimeters at the eastern North Honshu coast closest to Site M0090 (Ishimura and Hiramine, 2020) (Figure F1).

I targeted a sediment interval where a light reddish brown silt-sized tephra lens in Section 386-M0090D-1H-16 between 82.3 and 82.8 cm (Strasser et al., 2023a) has been identified as To-Cu ash

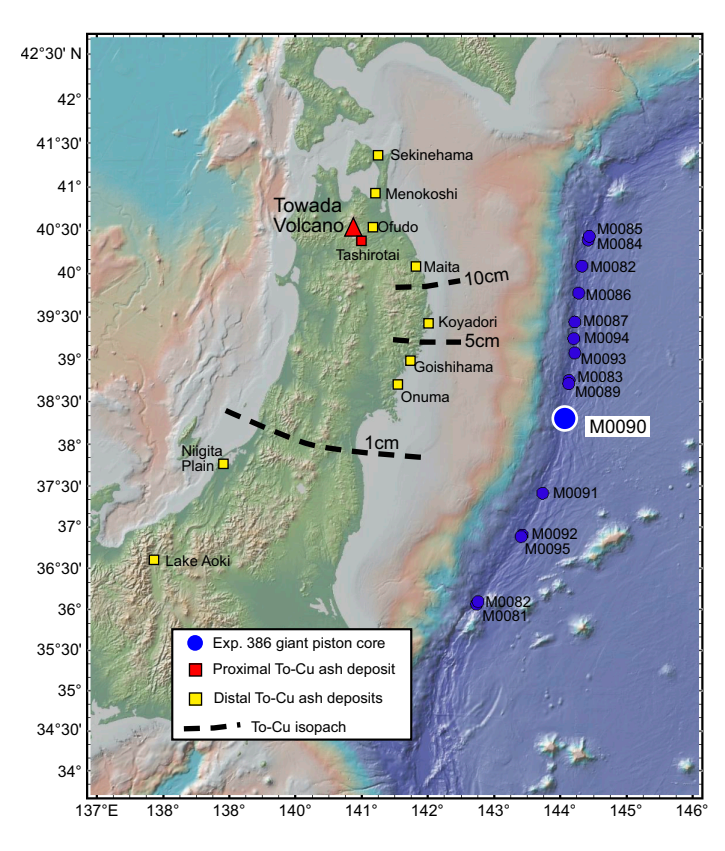


Figure F1. Location of giant piston cores in the Japan Trench offshore North Honshu, Expedition 386. Red triangle = Towada volcano with proximal outcrop of the To-Cu tephra (red square). Yellow squares = distal subaerial outcrop of the To-Cu tephra. To-Cu tephra locations and isopachs after Ishimura and Hiramine (2020). Map based on GeoMapApp.

bed (Satoguchi et al., 2024). This ash bed contains abundant pumiceous-type volcanic glass shards with fibrous and bubble-wall types, with subordinate brown volcanic glass shards (Strasser et al., 2023a). A problem, however, is that this To-Cu ash bed is contained within a ~130 cm thick layered deposit rich in silt and fine sand (Strasser et al., 2023a). This deposit has a sharp bottom at Section 1H-17, 30 cm, ~50 cm below the To-Cu bed, where magnetic susceptibility (MS) and bulk density abruptly increase and natural gamma radiation (NGR) decreases (Strasser et al., 2024). The latter three variables gradually return to their previous levels at the top of Section 1H-16 (0 cm), where, in addition, the silt and fine sand fractions decrease and the sediment becomes more clay rich again. In their entirety, these observations suggest that the ~130 cm thick coarse-grain sequence may have been deposited as a turbidite. Thus, the position of the identified To-Cu fallout bed at Section 1H-16, 83 cm, in the middle of this coarse-grain sequence raises concerns about whether the To-Cu tephra identified was indeed emplaced as a primary fallout deposit or whether the To-Cu tephra was entrained in a turbidite flow that accumulated during or after the To-Cu eruption in the Japan Trench basin.

To better understand the emplacement mode of the To-Cu tephra at Site M0090, I conducted high-resolution sampling with 1 or 5 cm spacing of sediment with a total thickness of 180 cm below and above the identified To-Cu marker bed for glass shards of dispersed tephra (dispersed tephra is not visible by the naked eye [Straub and Schmincke, 1998; Corry-Saavedra et al., 2019]) and analyzed the composition of the glass shards.

2. Materials and methods

2.1. Sample and sample preparation

Sediment samples were taken from two intervals in Holes M0090B and M0090D, where the presence of the To-Cu tephra was suspected based on preliminary results right after the shipboard sampling party in late 2022 (M. Strasser and K. Ikehara, pers. comm., 2022).

A lower stratigraphic section, 130 cm thick and composed of silt and fine sand, was sampled in Hole M0090B between Sections 1H-15, 80 cm (bottom), and 1H-14, 50 cm (top) (Figure F2). According to X-ray fluorescence (XRF) (Strasser et al., 2023a; Lin et al., 2024), this coarse-grained layered sequence correlates with the interval in Hole M0090D from Sections 1H-17, 30 cm (bottom), to 1H-16, 0 cm (top), where the To-Cu ash was identified in Section 1H-16, 83 cm (Satoguchi et al., 2024). Therefore, in Hole M0090B, the To-Cu ash is approximately located around Section 1H-15, 30 cm (Figure F2). According to Strasser et al. (2024), who used the composite core depth in meters below seafloor (mbsf), this section corresponds to the main part of the coarse-grained, graded, and silt- and sand-rich layers above tie-point C1-TP1 (see figure 9 in Strasser et al. [2024]).

Additionally, a stratigraphically higher, 50 cm thick interval was sampled in Section 386-M0090D-1H-15 between 50 cm (bottom) and 0 cm (top). In Hole M0090B, the stratigraphically higher interval is estimated to be located between Sections 1H-14, 0 cm (bottom), and 1H-13, 50 cm (top) (Figure F2). For this study, the stratigraphically lower and higher intervals were considered to represent a single stratigraphic column separated by an approximately 50 cm thick gap without samples. Hole-to-hole correlation might not be perfect on the millimeter scale, but it is sufficiently robust for this study.

The sediment column was sampled using six $2 \text{ cm} \times 2 \text{ cm}$ U-channels that were 30--40 cm long. Pieces of soft sediment, either 1 or 5 cm long, were cut from the U-channels with a spatula. Closer spaced samples (1 cm) were collected in intervals where the presence of To-Cu was initially suspected (Figure **F2**) before it was later identified in Section 386-M0090D-1H-16, 83 cm, by Satoguchi et al. (2024). A total of 65 samples were collected—47 from the lower interval and 18 from the higher interval—which include 35 samples of 1 cm thickness and 30 samples of 5 cm thickness. The samples are listed in Table **T1**.

The full sample volume was processed for the 1 cm samples; about half of the sample volume was processed for the 5 cm samples. The samples were freeze-dried and weighed before wet-sieving with tap water through single-use $27 \mu m$ polyester mesh screens to remove the clay and fine silt.

The coarser fraction >27 μ m was dried at ~40°C, weighted, and dry-sieved into >125 μ m, 63–125 μ m, and <63 μ m size fractions.

The >125 μ m fraction had rarely any lithogenic or biogenic particles except for fine sand-sized (>125–250 μ m) pumice particles found in the stratigraphically higher interval in Samples 386-M0090D-1H-15, 5–10 cm, and 1H-15, 10–15 cm. Sufficient volcanic glass shards and other volcanogenic and nonvolcanogenic particles (such as tests of diatoms and radiolaria) were found in the 63–125 μ m fraction. The 63–125 μ m fraction was mounted for microbeam analyses in its entirety without further separation to avoid fractionation of the glass shards, which is unavoidable when trying to separate silicic (rhyolitic) glasses from the silica tests.

Mount preparation for microbeam analyses followed the methods of Kutterolf et al. (2018). Several 1 inch diameter acrylic tablets with 12 holes of 4 mm diameter were used to mount 12 samples each. A small amount of the 63–125 μ m fraction was filled into the holes before filling with epoxy. The tablets were ground with 400 and 600 grit (American National Standards Institute [ANSI]) silicon carbide powder until ash particles of all 12 samples were sufficiently exposed before finishing the mount with 6 and 1 μ m diamond polish.

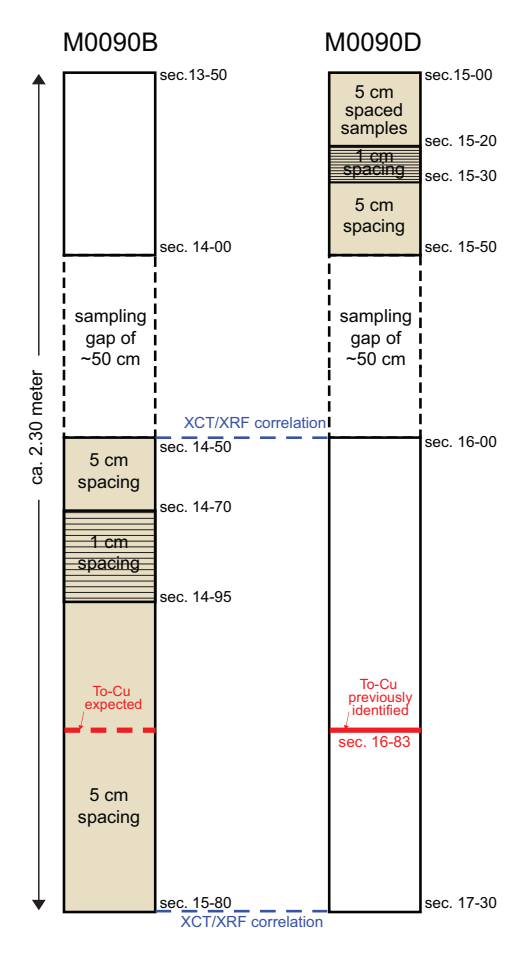


Figure F2. Composite of the ~230 cm thick stratigraphic section study at Site M0090, Holes M0090B and M0090D. Because of the different penetration depths of Holes M0090B and M0090D (Strasser et al., 2023b), identical stratigraphic intervals have different section numbers. Samples were taken from the lower interval in Hole M0090B and the higher interval in Hole M0090D (brown shading). These intervals are separated by a ~50 cm thick sample gap. The lower interval, which is rich in silt and fine sand, was correlated (blue dashes) using X-ray core tomography (XCT) (Strasser et al., 2023a) and XRF (Lin et al., 2024). The To-Cu ash is estimated to occur at 386-M0090B-1H-15, 30 cm, approximately corresponding to 386-M0090D-1H-16, 83 cm, where the To-Cu ash was recently identified by Satoguchi et al. (2024).

Table T1. Samples, together with percentages of the dry sediment fraction >27 μm, Holes M0090B and M0090D. **Download table in CSV format.**

Table T2. Electron microprobe analyses of glass shards, Holes M0090B and M0090D. Download table in CSV format.

Table T3. International glass standards for electron microprobe analyses of glass shards. Download table in CSV format.

2.2. Electron microprobe analysis

Electron microprobe analyses were carried out at the American Museum of Natural History (AMNH) in New York City (USA) with a Cameca SXFive Tactics microprobe analyzer equipped with five wavelength dispersive spectrometers. The sample mounts were carbon-coated before analysis. The acceleration voltage was 15 kV. A small beam diameter of 5 μm was enforced by the small area of exposed glass on the glass shards that are vesicular and often have microliths. Elements Si, K, and Na were measured with a 6 nA beam current, using LPET (K), LTAP (Na), and TAP (Si) crystals and peak counting times of 20 s (Si), 30 s (K), and 20 s (Na). Given the well-known loss of Na in silicic glass shards, the in-built t-zero mode was used to correct for Na loss. The t-zero method measures consecutively six peak/background ratios during the 20 s interval, which allows the determination of the Na loss rate (typically exponential) for a given data point. Na concentration was calculated by extrapolation of Na back to the time zero at the start of measurement (comparable to the backcounting method by Devine et al. [1995]). All other elements (Ti, Al, Mn, Fe, Mg, Ca, P, and Cl) were analyzed at 10 nA with a peak counting time of 45 s, except for Mg and Cl, which were counted for 90 s. A ZAF data reduction was carried out by means of the built-in PAP routine.

Typically, 10-15 glass shards per sample were analyzed. From a total of 800 individual electron microprobe analysis data points, 682 points (83%) were volcanic glass; the others hit other materials (biogenic silica, vesicles, microliths, inclusions, etc). Volcanic glass data were obtained from all 65 samples with an average of 10 ± 2 glass data points per sample.

Precision and accuracy of the major element oxides and Cl were monitored by the concurrent analyses of anhydrous and hydrous glasses. These include the basalt glass ML3B-G and the andesite glass StHS6/80-G from Jochum et al. (2006) and the in-house rhyolite glass BSB (Big Southern Butte) (J. Webster, pers. comm., 2024). The averages obtained compare well to the target values of long-term averages (Straub et al., 2024). There is no evidence of alkali loss in the anhydrous glass. Precision was monitored with a homogeneous but uncertified anhydrous rhyolite glass (RG) that closely matches the To-Cu glass composition. The averages for element oxides obtained from 48 data points and normalized to 100% are $SiO_2 = 77.3 \pm 0.42$ wt%, $CaO = 1.64 \pm 0.16$ wt%, and $K_2O = 2.13 \pm 0.04$ wt% with precisions (defined as percentage of one standard deviation of the average) of 0.6%, 3.3% and 1.8%, respectively (Tables **T2**, **T3**). Finally, a hydrous rhyolite glass chip (494) with an estimated 4.3 wt% H_2O (Devine et al., 1995) was used to monitor alkali stability and SiO_2 and Al_2O_3 ingrowth for hydrous glasses. Based on the target values given by Devine et al. (1995) and long-term averages of this glass chip (Straub et al., 2024), no evidence for instability/ingrowth for SiO_2 , Al_2O_3 , or K_2O was found. However, some Na_2O loss (up \sim 0.5 wt% absolute) seems to occur, which is not correctable by the t-zero mode at a beam current of 6 nA.

All electron microprobe data (samples and standards) are given in Tables T2 and T3.

3. Results

3.1. Identification of the To-Cu volcanic glasses

Volcanic glass shards observed are typically vesicular and colorless and include pumiceous frothy bubble wall shards. Sometimes the glasses contain microliths. All glass shards are rhyolitic with $SiO_2 > 71$ wt% when normalized to 100% sum of oxides (Figure F3). The K_2O concentrations vary widely from low-K (\sim 1.4 wt% K_2O) to high-K (\sim 5 wt% K_2O) compositions (Figure F3A). In the CaO versus K_2O space, two compositional groups of the Site M0090 glasses can be distinguished (Figure F3B) by the simple means of separating the glasses into a low- K_2O (<1.5 wt%) and high- K_2O (<1.5 wt%) group.

The low- K_2O group comprises 67% of the glasses measured. It has comparatively higher CaO, FeO*, and TiO₂ concentrations. Low-K glasses form a tight trend in the CaO versus K_2O space, which matches very well those of the glasses from the To-Cu eruption found at the distal sites across North Honshu (Ishimura and Hiramine, 2020). Other major element oxides also match but do not discriminate as well between the K-rich and low-K glasses. Although small deviations occur (e.g., a seemingly higher TiO₂ in the distal To-Cu glasses), these seem rather attributable to interlaboratory bias than to actual differences. Thus, I propose that the Site M0090 low-K glasses originate from explosive eruptions of the Towada volcano.

To further assess the similarities between the Site M0090 low-K glasses and the distal To-Cu glasses shards, which are extensively investigated (Ishimura and Hiramine, 2020), their CaO distribution is compared in Figure **F4**.

The Site M0090 low-K glasses show a very similar abundance distribution to the distal To-Cu glasses from Ishimura and Hiramine (2020), which supports (but does not prove) a common origin. However, the Site M0090 low-K glasses also exhibit a tail of lower CaO glasses, which have not been observed within the distal, subaerial To-Cu glasses (Ishimura and Hiramine, 2020). The glasses in the low-CaO tail also have slightly lower FeO and very slightly higher K₂O than reported from distal subaerial To-Cu glasses. However, such low-K, low-CaO glasses are typically present in older and younger eruptions of Towada (Ishimura, 2024). Thus, although the low-K glasses are in all likelihood from Towada volcano, they may not exclusively represent the To-Cu eruption, or may even originate from other explosive Towada eruptions.

3.2. Emplacement mode

The Site M0090 low-K and K-rich glasses are plotted against section depth in Figure **F5**. Both glass types are present in each sample of the lower and higher stratigraphic sections. Based on the compositional data collected, there is no horizon recognizable where the low-K glasses are more strongly concentrated in such a way that an instantaneous fallout event was marked. The only stratigraphic change occurs in the number of glass shards analyzed from low-K and K-rich glasses,

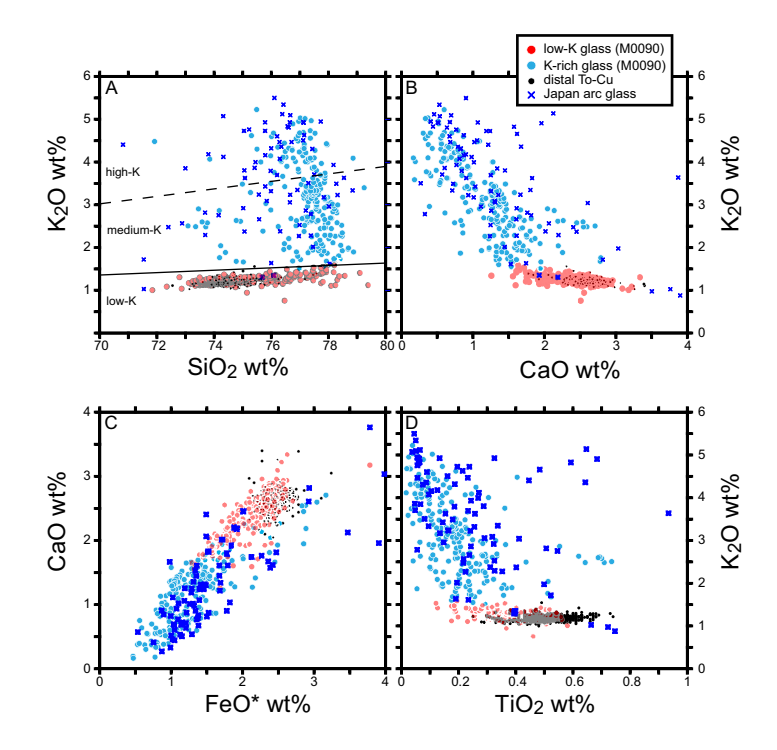


Figure F3. Major element oxides of glass shard compositions, Site M0090, compared to the glasses of the distal To-Cu sites (Ishimura and Hiramine, 2020) and the Japan arc (Kimura et al., 2015). All glass composition normalized to 100% sum of oxides. A. K₂O vs. SiO₂ with division into K-series after Le Maitre (1989). B. K₂O vs. CaO. C. CaO vs. FeO*. D. K₂O vs. TiO₂ after Aoki and Machida (2006).

which varies with depth: the low-K glasses are most abundant in the lowermost part and then slightly decrease with decreasing section depth, and the K-rich glasses become more frequent at the same time. Moreover, in the stratigraphically higher interval, the count is reversed, with fewer low-K glasses analyzed than K-rich glasses.

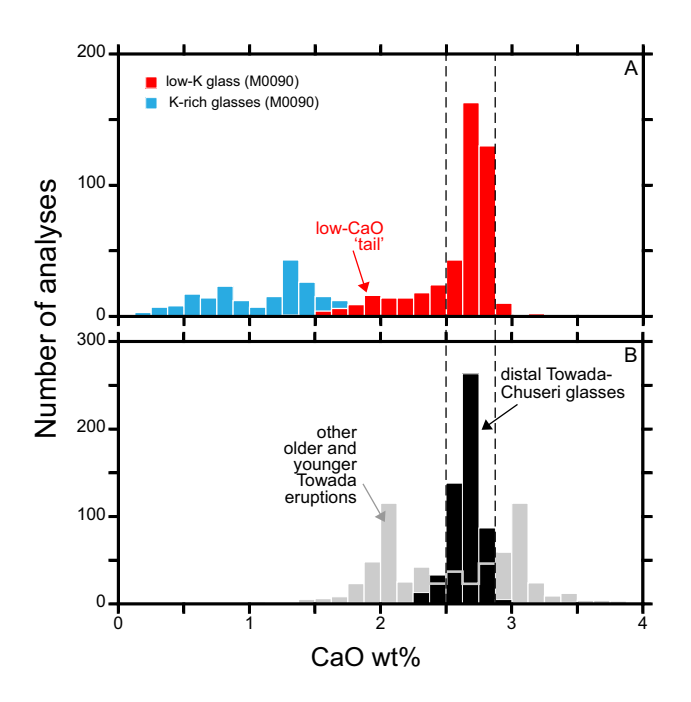


Figure F4. CaO wt%. A. Site M0090 glasses. B. Distal To-Cu glasses (Ishimura and Hiramine, 2020) compared to glasses produced during early and later explosive eruptions of the Towada volcano (Ishimura, 2024).

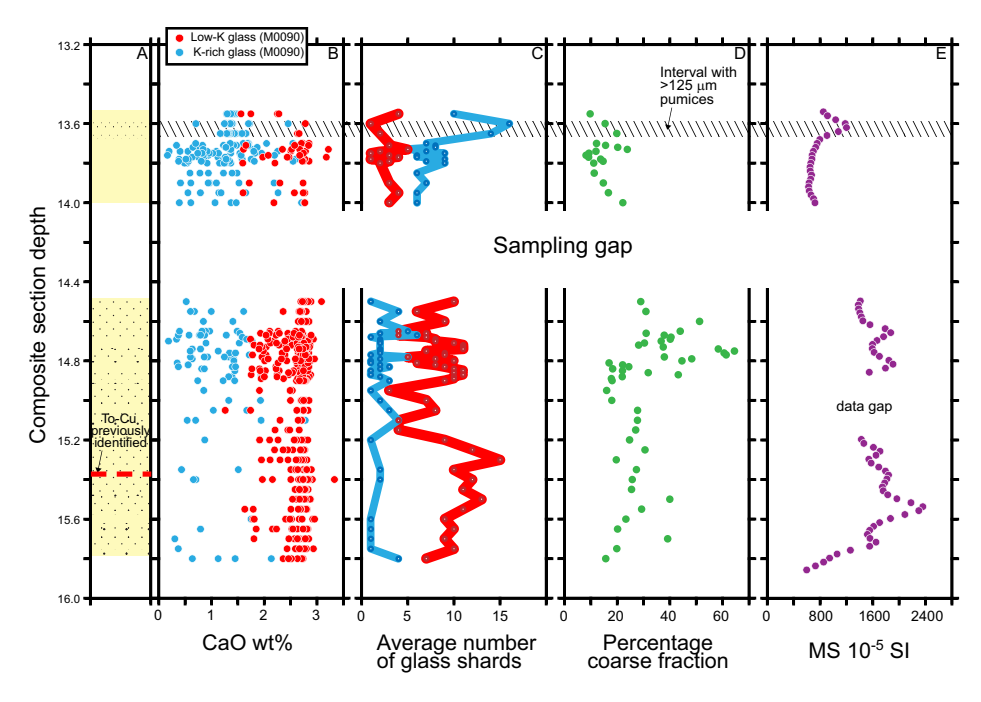


Figure F5. Depth distribution of low-K and K-rich glasses, Site M0090. A. Layers of silt and very fine sand in clayey sediment; B. CaO of low-K and K-rich glasses. C. Average number of low-K and K-rich glasses identified in each sample by electron microprobe analyses. Note abundance reversal in the stratigraphically higher interval where low-K glasses are rarer than K-rich glasses. D. Weight percentage of coarse fraction >27 μ m in individual samples. E. MS from Strasser et al. (2025a; 2025b). The To-Cu ash bed previously identified by Satoguchi et al. (2024) is indicated. Pumice particles >125 μ m have K-rich compositions (~3 wt% K_2 O) (see Table T2 for glass shards denoted with a P).

The reversal in the abundances of the glass compositional type is paralleled by a slight overall decrease in the percentage of the coarser (>27 μ m) sediment fraction with decreasing stratigraphic depth. The highest percentages of the coarser (>27 μ m) fraction are reported from an interval where samples are spaced 1 cm apart and where the centimeter-scale grain size variations may be better resolved. The trend and fluctuations of MS are consistent with these variations, which suggests that grain size and coarser particle load decrease with decreasing depth.

No sample was taken below the coarse-grained layered sediment sequence. Thus, it remains open whether the low-K glass distribution drops below the base of the coarse-grained layered sediment sequence or even disappears altogether with increasing core depth. All the same, the persistent presence of low-K and K-rich glasses throughout the coarse-grained layered sediment sequence suggests that they were emplaced as part of this entire sequence and not as discrete layers of either type. It is possible that the coarse-grained layered sediment was deposited from a turbidite mass flow, which typically has a finely layered structure due to variations in grain size and componentry. Possibly, the previously identified lenticular layer of To-Cu airfall ash marks a thin lamina where (low-K) glasses are sufficiently concentrated to become visible to the naked eye.

It is possible that the rapid deposition of airborne ash from an explosive Towada eruption onto the steep submarine continental slope triggered downslope flow into the trench. Entrainment of older sediment from the slope surface, including tephra glasses from previous K-rich and Towada eruptions, may then account for the presence of multiple glass populations in the sediment sequence investigated.

4. Acknowledgments

This research used samples and data provided by IODP. IODP curator Yusuke Kubo and his staff at the IODP Kochi Core Center in Japan are thanked for taking the U-channels of Site M0090 cores. Celine Martin is thanked for her support with the electron microprobe work at the AMNH. Comments from reviewer Daisuke Ishimura and editor Ken Ikehara improved this report. Funding for this research was provided by a USSSP Post-Expedition Activity award grant to S.M. Straub.

References

- Aoki, K., Irino, T., and Oba, T., 2008. Late Pleistocene tephrostratigraphy of the sediment core MD01-2421 collected off the Kashima coast, Japan. The Quaternary Research (Daiyonki-Kenkyu), 47(6):391–407. https://doi.org/10.4116/jaqua.47.391
- Aoki, K., and Machida, H., 2006. Major element composition of volcanic glass shards in the late Quaternary widespread tephras in Japan – distinction of tephras using K₂O-TiO₂ diagrams. Bulletin of the geological Survey of Japan, 57(7–8):239–258. https://doi.org/10.9795/bullgsj.57.239
- Corry-Saavedra, K., Schindlbeck, J.C., Straub, S.M., Murayama, M., Bolge, L.L., Gómez-Tuena, A., Hashimoto, Y., and Woodhead, J.D., 2019. The role of dispersed ash in orbital-scale time-series studies of explosive arc volcanism: insights from IODP Hole U1437B, Northwest Pacific Ocean. International Geology Review, 61(17):2164–2183. https://doi.org/10.1080/00206814.2019.1584770
- Devine, J.D., Gardner, J.E., Brack, H.P., Layne, G.D., and Rutherford, M.J., 1995. Comparison of microanalytical methods for estimating H₂O contents of silicic volcanic glasses. American Mineralogist, 80(3–4):319–328. https://doi.org/10.2138/am-1995-3-413
- Ikehara, K., Usami, K., Kanamatsu, T., Danhara, T., and Yamashita, T., 2017. Three important Holocene tephras off the Pacific coast of the Tohoku region, Northeast Japan: Implications for correlating onshore and offshore event deposits. Quaternary International, 456:138–153. https://doi.org/10.1016/j.quaint.2017.08.022
- Ishimura, D., 2024. Major element composition of volcanic glass shards in the late Quaternary tephras from the Towada volcano, Northeast Japan. Geographical Reports of Tokyo Metropolitan University, 59:135–142. https://hdl.handle.net/10748/0002000572
- Ishimura, D., and Hiramine, R., 2020. Proximal—distal fall deposit correlation of VEI-5 tephra (Towada-Chuseri) from Towada volcano, northeast Japan. Journal of Quaternary Science, 35(1–2):334–348. https://doi.org/10.1002/jqs.3161
- Jochum, K.P., Stoll, B., Herwig, K., Willbold, M., Hofmann, A.W., Amini, M., Aarburg, S., Abouchami, W., Hellebrand, E., Mocek, B., Raczek, I., Stracke, A., Alard, O., Bouman, C., Becker, S., Dücking, M., Brätz, H., Klemd, R., de Bruin, D., Canil, D., Cornell, D., de Hoog, C.-J., Dalpé, C., Danyushevsky, L., Eisenhauer, A., Gao, Y., Snow, J.E., Groschopf, N., Günther, D., Latkoczy, C., Guillong, M., Hauri, E.H., Höfer, H.E., Lahaye, Y., Horz, K., Jacob, D.E., Kasemann, S.A., Kent, A.J.R., Ludwig, T., Zack, T., Mason, P.R.D., Meixner, A., Rosner, M., Misawa, K., Nash, B.P., Pfänder, J., Premo, W.R., Sun, W.D., Tiepolo, M., Vannucci, R., Vennemann, T., Wayne, D., and Woodhead, J.D.,

- 2006. MPI-DING reference glasses for in situ microanalysis: New reference values for element concentrations and isotope ratios. Geochemistry, Geophysics, Geosystems, 7(2):Q02008. https://doi.org/10.1029/2005GC001060
- Kimura, J.-I., Nagahashi, Y., Satoguchi, Y., and Chang, Q., 2015. Origins of felsic magmas in Japanese subduction zone: Geochemical characterizations of tephra from caldera-forming eruptions <5 Ma. Geochemistry, Geophysics, Geosystems, 16(7):2147–2174. https://doi.org/10.1002/2015GC005854
- Kutterolf, S., Schindlbeck, J.C., Robertson, A.H.F., Avery, A., Baxter, A.T., Petronotis, K., and Wang, K.-L., 2018. Tephrostratigraphy and provenance From IODP Expedition 352, Izu-Bonin Arc: tracing tephra sources and volumes from the Oligocene to Recent. Geochemistry, Geophysics, Geosystems, 19(1):150–174. https://doi.org/10.1002/2017GC007100
- Le Maitre, R.W., 1989. A Classification of Igneous Rocks and Glossary of Terms: Boston (Blackwell).
- Lin, J.-T., Huang, J.J., Ikehara, K., Strasser, M., Hsu, T.W., Su, C.C., 2024. Chemical-based event-stratigraphic correlation in the central Japan Trench by XRF-CS chemical fingerprint and multivariate statistics. Presented at the IODP Expedition 386 2nd Post-Cruise Meeting, Anchorage, Alaska.
- Machida, H., 1999a. Quaternary widespread tephra catalog in and around Japan: recent progress. The Quaternary Research (Daiyonki-Kenkyu), 38(3):194–201. https://doi.org/10.4116/jaqua.38.194
- Machida, H., 1999b. The stratigraphy, chronology and distribution of distal marker-tephras in and around Japan. Global and Planetary Change, 21(1–3):71–94. https://doi.org/10.1016/S0921-8181(99)00008-9
- Machida, H., 2002. Volcanoes and tephras in the Japan area. Global Environmental Research, 6(2):19–28. https://airies.wikiplus.net/attach.php/6a6f75726e616c5f30362d32656e67/save/0/0/06_2-03.pdf
- Matsu'ura, T., and Komatsubara, J., 2018. Detection of Late Pleistocene tephras and cryptotephras using major element chemistry of glass shards from Chikyu C9001C cores, NW Pacific Ocean. JAMSTEC Report of Research and Development, 26:1–20. https://doi.org/10.5918/jamstecr.26.1
- McLean, D., Albert, P.G., Nakagawa, T., Suzuki, T., Staff, R.A., Yamada, K., Kitaba, I., Haraguchi, T., Kitagawa, J., and Smith, V.C., 2018. Integrating the Holocene tephrostratigraphy for East Asia using a high-resolution cryptotephra study from Lake Suigetsu (SG14 core), central Japan. Quaternary Science Reviews, 183:36–58. https://doi.org/10.1016/j.quascirev.2017.12.013
- Newhall, C.G., and Self, S., 1982. The volcanic explosivity index (VEI) an estimate of explosive magnitude for historical volcanism. Journal of Geophysical Research: Oceans, 87(C2):1231–1238. https://doi.org/10.1029/JC087iC02p01231
- Satoguchi, Y., Nagahashi, Y., and Ikehara, K., 2024. Tephra correlations between the sites under the Japan Trench. Presented at the IODP Expedition 386 2nd Post-Cruise Meeting, Anchorage, Alaska.
- Strasser, M., Ikehara, K., Everest, J., Maeda, L., Hochmuth, K., Grant, H., Stewart, M., Okutsu, N., Sakurai, N., Yokoyama, T., Bao, R., Bellanova, P., Brunet, M., Cai, Z., Cattaneo, A., Hsiung, K.-H., Huang, J.-J., Ishizawa, T., Itaki, T., Jitsuno, K., Johnson, J.E., Kanamatsu, T., Keep, M., Kioka, A., Kölling, M., Luo, M., März, C., McHugh, C., Micallef, A., Nagahashi, Y., Pandey, D.K., Proust, J.-N., Rasbury, E.T., Riedinger, N., Satoguchi, Y., Sawyer, D.E., Seibert, C., Silver, M., Straub, S.M., Virtasalo, J., Wang, Y., Wu, T.-W., and Zellers, S.D., 2023a. Site M0090 (Basin C1). In Strasser, M., Ikehara, K., Everest, J., and the Expedition 386 Scientists, Japan Trench Paleoseismology. Proceedings of the International Ocean Discovery Program, 386: College Station, TX (International Ocean Discovery Program). https://doi.org/10.14379/iodp.proc.386.106.2023
- Strasser, M., Ikehara, K., Everest, J., and the Expedition 386 Scientists, 2023b. Japan Trench Paleoseismology. Proceedings of the International Ocean Discovery Program, 386: College Station, TX (International Ocean Discovery Program). https://doi.org/10.14379/iodp.proc.386.2023
- Strasser, M., Ikehara, K., Everest, J.D., Maeda, L., Hochmuth, K., Grant, H., Stewart, M.S., Sakurai, N., Yokoyama, T., Bao, R., Bellanova, P., Brunet, M., Cai, Z., Cattaneo, A., Hsiung, K.-H., Huang, J.-J.S., Ishizawa, T., Itaki, T., Jitsuno, K., Johnson, J.E., Kanamatsu, T., Keep, M., Kioka, A., Kölling, M., Luo, M., März, C., McHugh, C.M.G., Micallef, A., Nagahashi, Y., Pandey, D.K., Proust, J.-N., Rasbury, T., Riedinger, N., Satoguchi, Y., Sawyer, D.E., Seibert, C., Silver, M., Straub, S.M., Virtasalo, J.J., Wang, Y.H., Wu, T.-W., and Zellers, S.D., 2025a. Physical properties (MSCL) of IODP Hole 386-M0090B. https://doi.org/10.1594/PANGAEA.974931
- Strasser, M., Ikehara, K., Everest, J.D., Maeda, L., Hochmuth, K., Grant, H., Stewart, M.S., Sakurai, N., Yokoyama, T., Bao, R., Bellanova, P., Brunet, M., Cai, Z., Cattaneo, A., Hsiung, K.-H., Huang, J.-J.S., Ishizawa, T., Itaki, T., Jitsuno, K., Johnson, J.E., Kanamatsu, T., Keep, M., Kioka, A., Kölling, M., Luo, M., März, C., McHugh, C.M.G., Micallef, A., Nagahashi, Y., Pandey, D.K., Proust, J.-N., Rasbury, T., Riedinger, N., Satoguchi, Y., Sawyer, D.E., Seibert, C., Silver, M., Straub, S.M., Virtasalo, J.J., Wang, Y.H., Wu, T.-W., and Zellers, S.D., 2025b. Physical properties (MSCL) of IODP Hole 386-M0090D. https://doi.org/10.1594/PANGAEA.974933
- Strasser, M., Ikehara, K., Pizer, C., Itaki, T., Satoguchi, Y., Kioka, A., McHugh, C., Proust, J.-N., Sawyer, D., and the IODP 386 Expedition Management Team, 2024. Japan Trench event stratigraphy: first results from IODP giant piston coring in a deep-sea trench to advance subduction zone paleoseismology. Marine Geology, 477:107387. https://doi.org/10.1016/j.margeo.2024.107387
- Straub, S.M., Reilly, B., Raymo, M.E., Gómez-Tuena, A., Wang, K.-L., Widom, E., Kuentz, D., and Arculus, R.J., 2024. Patterns of Plio-Pleistocene ice volume variability recorded by the large-magnitude explosive eruptions from the Kamchatka-Kurile Volcanic Arc. Geochemistry, Geophysics, Geosystems, 25(10):e2024GC011748. https://doi.org/10.1029/2024GC011748
- Straub, S.M., and Schmincke, H.U., 1998. Evaluating the tephra input into Pacific Ocean sediments: distribution in space and time. International Journal of Earth Sciences, 87(3):461–476. https://doi.org/10.1007/s005310050222
- Sun, C., Plunkett, G., Zhu, Z., Zhang, L., Zhang, B., Zhang, D., Mao, Q., You, H., Wang, L., Chu, G., and Liu, J., 2021. ~5.9 cal ka bp Towada-Chuseri tephra from Towada volcano: a mid-Holocene marker layer from Japan to northeast China. Journal of Quaternary Science, 36(7):1143–1148. https://doi.org/10.1002/jqs.3362